IJCAT - International Journal of Computing and Technology, Volume 3, Issue 1, January 2016
ISSN : 2348 - 6090
www.IJCAT.org

HVAC Transmission for Offshore Wind Power

[1] T. Rajesh, [2] M. Chandra Sekhar

[1] M. Tech Student Lenora College of Engineering- Rampachodavaram

[2] Asst. Professor, Lenora College of Engineering- Rampachodavaram

Abstract - This paper presents a low-frequency ac (LFAC) transmission system for offshore wind power. The LFAC system is interfaced with the main power grid with a cycloconverter. The wind power plant collection system is dc based, and connects to the LFAC transmission line with a 12-pulse thyristor converter. The main advantage of the LFAC technology is the increase of power capacity and transmission distance for a given submarine cable compared to 50-Hz or 60-Hz HVAC. This leads to substantial cost savings due to the reduction in cabling requrments (i.e, less lines in parallel for a desired power level) and the use of normal AC breakers for protection. A method to design the system's components and controls is set forth. Simulation results are provided to illustrate the system's performance.

Keywords **- Power Transmission, Thyristor Converters, Under-Water Power Cables, Wind Energy.**

1. Introduction

OFFSHORE wind power plants are expected to represent a signific ant component of the future electric generation portfolio due to greater space availability and better wind energy potential in offshore locations [1], [2]. The integration of offshore wind power plants with the main power grid is a subject of ongoing research [3]–[5]. Presently, high-voltage ac (HVAC) and high-voltage dc (HVDC) are well-established technologies for transmission [6]. HVAC transmission is advantageous because it is relatively straightforward to design the protection system and to change voltage levels using transformers. However, the high capacitance of submarine ac power cables leads to considerable charging current, which, in turn, reduces the active power transmission capacity and limits the transmission distance. HVAC is adopted for relatively short (up to 50–75 km) underwater transmission distances [Two classes of HVDC systems exist, depending on the types of power-electronic devices used:

1) line-commutated converter
HVDC (LCC-HVDC) using thyristors and

2) voltage-source converter HVDC (VSC-HVDC) using self-commutated devices, for example, insulated-gate bipolar transistors (IGBTs) [8]. The main advantage of HVDC technology is that it imposes essentially no limit on transmission distance due to the absence of reactive current in the transmission line [9].

LCC-HVDC systems are capable of handling power up to 1 GW with high reliability [7]. LCCs consume reactive power from the ac grid and introduce low-order harmonics, which inevitably results in the requirement for auxiliary equipment, such as capacitor banks, ac filters, and static synchronous compensators [4]. On the other hand, VSC-HVDC systems are able to independently regulate active and reactive power exchanged with the onshore grid and the offshore ac collection grid. The reduced efficiency and cost of the converters can be identified as drawbacks of VSC-HVDC systems [6]. Power levels (typically on the order of 300–400 MW) and reliability are lower than those of LCC-HVDC [7], [9]. HVDC is applied for distances greater than 100 km for offshore wind power transmission.

Besides HVAC and HVDC, high-voltage low-frequency ac (LFAC) transmission has been recently proposed [10]–[13]. In LFAC systems, an intermediate-frequency level is used, which is created using a cycloconverter that lowers the grid frequency to a smaller value, typically to one-third its value. In general, the main advantage of the LFAC technology is the increase of power capacity and transmission distance for a given submarine cable compared to 50-Hz or 60-Hz HVAC. This leads to substantial cost savings due to the reduction in cabling requirements (i.e., less lines in parallel for a desired power level) and the use of normal ac breakers for protection.

In this paper, a novel LFAC transmission topology is analyzed. The proposed system differs from previous work [11]–[13] in that the wind turbines are assumed to be interconnected with a medium-voltage (MV) dc grid, in

contrast with current practice, where the use of MV ac collection grids is standard [14]. DC collection is becoming a feasible alternative with the development of cost-effective and reliable dc circuit breakers [15], and studies have shown that it might be advantageous with respect to ac collection in terms of efficiency and improved production costs [16].

The required dc voltage level can be built by using high-power dc–dc converters [17], [18] and/or by the series connection of wind turbines [19]–[22]. For example, multi-MW permanent-magnet synchronous generators with fully rated power converters (Type-4 turbines) are commonly used in offshore wind plants. By eliminating grid-side inverters, a medium-voltage dc collection system can be formed by interconnecting the rectified output of the generators [23].

The main reason for using a dc collection system with LFAC transmission is that the wind turbines would not need to be redesigned to output low-frequency ac power, which would lead to larger, heavier, and costlier magnetic components (e.g., step-up transformers and generators). The design of the dc collection system is outside the scope of this paper.

At the sending end of the proposed LFAC system, a dc/ac 12-pulse thyristor-based inverter is used to generate low-frequency (20- or 16 2/3-Hz) ac power, as shown in Fig. 1. At the onshore substation (the receiving end), a thyristor-based cycloconverter is used as an interface between the low-frequency side and the 60- or 50-Hz onshore power grid.

Thyristor-based converters can transmit more power with increased reliability and lower cost compared to VSC-HVDC systems. However, large filters are necessary at both ends to suppress low-order harmonics and to supply reactive power. Furthermore, the system can be vulnerable to main power grid disturbances.

The proposed LFAC system could be built with commercially available power system components, such as the receiving-end transformers and submarine ac cables designed for regular power frequency. The phase-shift transformer used at the sending end could be a 60-Hz transformer derated by a factor of three, with the same rated current but only one-third of the original rated voltage. Another advantage of the proposedLFAC scheme is its feasibility for ultiterminal transmission, since the design of multiterminal HVDC is complicated [24], [25], but the analysis of such an application is not undertaken herein. In summary, LFAC transmission could be an attractive technical solution for medium-distance transmission (i.e., in between HVAC and HVDC) [12].

The objective of this paper is to set forth as a design process for an LFAC system for point-to-point transmission. The system configuration and control strategies are outlined in Section II. The selection of the major system components is discussed in Section III-A, and filter design is discussed in Section III-B. A design example and time-domain simulation study of the proposed LFAC system are provided in Sections IV and V, respectively. Section VI concludes this paper.

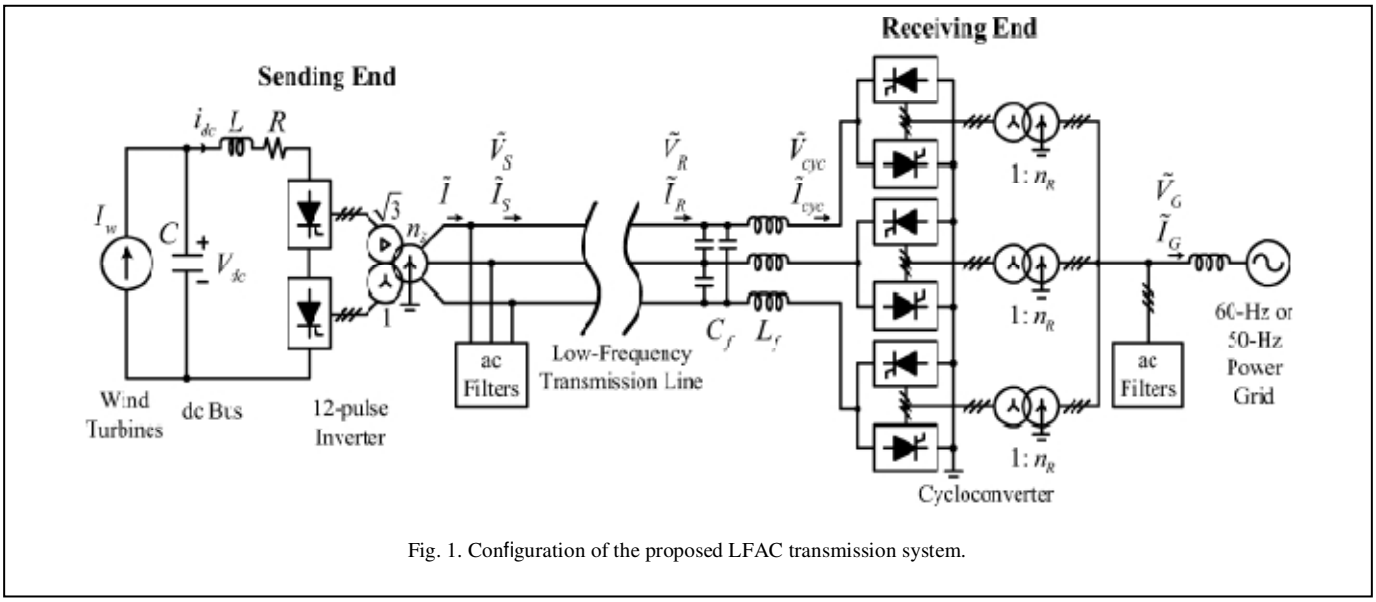

Fig. 1. Configuration of the proposed LFAC transmission system.

2. System Configuration and Control

The proposed LFAC transmission system is shown in Fig. 1, assuming a 60-Hz main grid. At the sending end, a medium-voltage dc collection bus is formed by rectifying the ac output power of series-connected wind turbines [16]. A dc current source represents the total power delivered from the wind turbines. A dc/ac 12-pulse thyristor-based inverter is used to convert dc power to low-frequency (20-Hz) ac power.

It is connected to a three-winding transformer that raises the voltage to a higher level for transmission. AC filters are used to suppress the 11th, 13th, and higher-order (23rd) current harmonics, and to supply reactive power to the converter. A smoothing reactor is connected at the dc terminals of the inverter. At the receiving end, a three-phase bridge (6-pulse) cycloconverter is used to generate 20-Hz voltage. A filter is connected at the low-frequency side. At the grid side, ac filters are used to suppress odd current harmonics, and to supply reactive power to the cycloconverter. Simply put, the operation of the LFAC transmission system can be understood to proceed as follows. First, the cycloconverter at the receiving end is activated, and the submarine power cables are energized by a 20-Hz voltage. In the meantime, the dc collection bus at the sending end is charged using power from the wind turbines. After the 20-Hz voltage and the dc bus voltage are established, the 12-pulse inverter at the sending end can synchronize with the 20-Hz voltage, and starts the transmission of power. In reality, more sophisticated schemes for system startup would have to be devised, based nevertheless on this operating
principle.

A. Sending-End Control

The control structure for the sending-end inverter is shown in Fig. 2. The controller regulates the dc bus voltage V_{dc} by adjusting the voltage Vac at the inverter terminals. The cosine wave crossing method [26] is applied to determine the firing angle

$$\alpha_S = \arccos\left(\frac{V^*}{V_P}\right)$$

Where Vp is the peak value of the cosine wave. Note that $V^*<0$ and $90^0<a_s<180^0$ (using common notation), since the converter is in the inverter mode of operation [27].V and Vs (line-to-neutral, rms) are related by [28]

$$V = \frac{6\sqrt{6}V_S}{\pi n_S}\cos(\alpha_S).$$

A phase-locked loop (PLL) provides the angular position of the ac-side voltage, which is necessary for generating the firing pulses of the thyristors. It also outputs the rms value of theundamental component of the voltage, which is used in the firing-angle calculation.

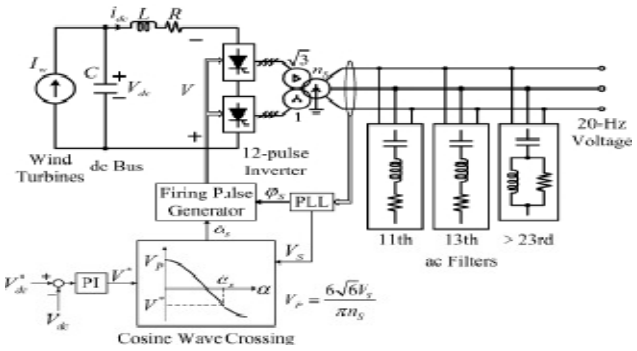

Fig. 2. Sending-end inverter control.

B. Receiving-End Control

The structure of the cycloconverter controller at the receiving end is illustrated in Fig. 3. The control objective is to provide a constant 20-Hz voltage1 of a given rms value V^*_{cyc} (line-to-neutral). The fundamental component of the cycloconverter voltage Vcyc is obtained with the signal conditioning logic depicted in Fig. 4.

The firing angles are determined with the cosine wave crossing method, as shown in Fig. 5, which uses phase- as an example. The firing angles of the phase-a positive and negative converters (denoted as "*aP*" and "*aN*" in Fig. 3) are α_sP and α_aN , respectively. For the positive converter, the average voltage at the 20-Hz terminals is given by [28]

$$V_{aP} = \frac{3\sqrt{6}V_G}{\pi n_R}\cos(\alpha_{aP})$$

where V_G is the rms value of the line-to-neutral voltage at the grid side, η_B and is the turns ratio of the transformers. The condition α_sP+ α_aN=π ensures that average voltages with the same polarity are generated from the positive and negative converter at the 20-Hz terminals [30]. The firing pulses and are not simultaneously applied to both converters, in order to obtain a noncirculating current mode of operation. This functionality is embedded in the "Bank Selector" block of Fig. 3, which operates based on the filtered current Icyc.abc. Note (for later use) that the maximum line-to-neutral rms value of the 20-Hz cycloconverter voltage is [26] and that a voltage ratio is defined as

$$V_{cyc}^{max} = \frac{3\sqrt{3}V_G}{\pi n_R} \qquad r = \frac{V_{cyc}}{V_{cyc}^{max}}$$

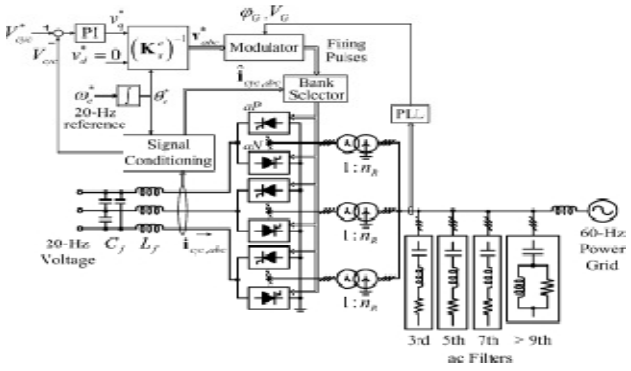

Fig. 3. Receiving-end cycloconverter control. (The reference frame transformation matrix is defined in [29], and transforms variables from the stationary to the synchronous reference frame.)

In practice, the theoretical maximum value γ= 1 cannot be achieved, due to the leakage inductance of the transformers, which was ignored in the analysis.

3. System Design

3.1 Main Power Components

The main power components are selected based on a steadystate analysis of the LFAC transmission system shown in Fig. 1, under the following assumptions:

- Only fundamental components of voltages and currents are considered. The receiving end is modeled as a 20-Hz voltage source of nominal magnitude.
- The power losses of the reactor, thyristors, filters, and transformers are ignored.
- The resistances and leakage inductances of transformers are neglected.
- The ac filters are represented by an equivalent capacitance corresponding to the fundamental frequency.
- The design is based on rated operating conditions (i.e.,maximum power output).

At the steady state, the average value of the dc current is Idc equal to Iw, so the power delivered from the wind turbines is

$$P_w = V_{dc} I_w.$$

For the 12-pulse converter, the rms value of the current at the transmission side is [28]

$$I = \frac{2\sqrt{6}}{\pi} \frac{I_w}{n_S}.$$

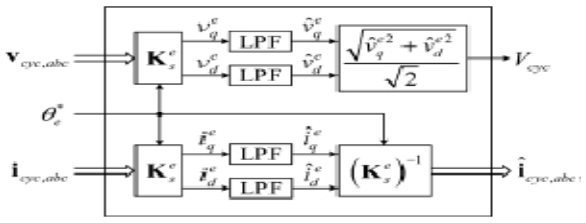

Fig. 4. Details of the signal conditioning block

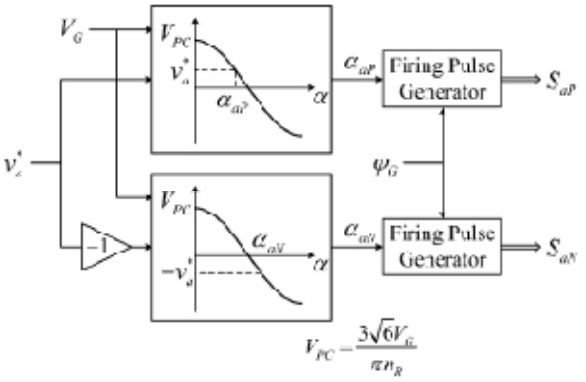

Fig. 5. Modulator for phase .

Hence, (7) can be written as

$$I = MP_w \quad \text{with}$$

$$M = \frac{2\sqrt{6}}{\pi n_S V_{dc}}.$$

Let $\bar{V}_S = V_S \angle 0°$ and denote the phasors of the line-toneutral voltage and line current, respectively. Since $-\bar{I}$ lags $\bar{V}_S$ by α_S [28], it follows that $\bar{I} = I \angle 180° - \alpha_S$. The active power delivered by the 12-pulse inverter is given by

$$P_S = P_w = 3V_S I \cos(\alpha_S - 180°) = -3V_S I \cos(\alpha_S) > 0. \quad (10)$$

Substitution 8 into 10

$$\cos(\alpha_S) = -\frac{1}{3MV_S}$$

$$\sin(\alpha_S) = \sqrt{1 - \frac{1}{9M^2 V_S^2}}.$$

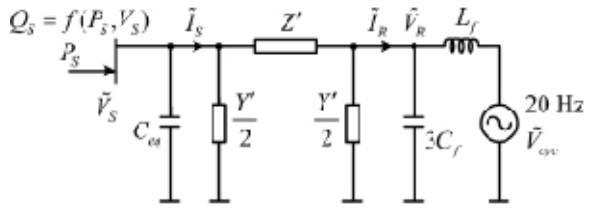

Fig. 6. Equivalent circuit of the LFAC transmission system at fundamental frequency.

The reactive power generated from the 12-pulse inverter is

$$Q_S = 3V_S I \sin(\alpha_S - 180°) = -3V_S I \sin(\alpha_S). \quad (13)$$

From 10-3

$$Q_S = P_S \tan(\alpha_S) = -P_S\sqrt{9M^2V_S^2 - 1}. \quad (14)$$

The negative sign in (13) and (14) indicates that the 12-pulse inverter always absorbs reactive power. Equation (14) shows that Qs can be expressed as a function Qs=$f(Ps, Vs)$

Based on the aforementioned analysis, the steady-state single-phase equivalent circuit of the LFAC transmission system is shown in Fig. 6. The equivalent capacitance of the sending-end ac filters at the fundamental frequency is Ceq . The transmission line is modeled by a π-equivalent (positive-sequence) circuit using lumped parameters. The well-known hyperbolic trigonometric expressions for Z' and Y'/2 are used [31]. Given a power rating of a wind power plant Prated , the maximum reactive power that is absorbed by the 12-pulse inverter can be estimated according to (14), which yields

$$Q_{\text{rated}} = P_{\text{rated}}\sqrt{3M^2V_c^2 - 1} \quad (15)$$

Where V_0 is the nominal transmission voltage level (line-to-line rms).Here, it is assumed that the sending-end ac filters supply the rated reactive power to the inverter. Therefore

$$C_{\text{eq}} = \frac{Q_{\text{rated}}}{\omega_e V_c^2} \quad (16)$$

where rad/s. In addition, the apparent power rating of the transformer at the sending end should satisfy

$$S_{tS} > \sqrt{P_{\text{rated}}^2 + Q_{\text{rated}}^2} = \sqrt{3}P_{\text{rated}}MV_o. \quad (17)$$

At the 60-Hz grid side, the reactive power capacity of the ac filters and the apparent power rating of the transformers depend on the cycloconverter's voltage ratio , which is a design parameter, and the 20-Hz side power factor [30], which can be estimated as follows. For a given transmission cable, the voltage ratings (nominal and maximum voltage), the current rating, and the distributed cable parameters (resistance, inductance, and capacitance per unit length) are known. Here, it is assumed that a power cable is chosen to transmit the rated wind power plant power P without violating the cable's voltage and current ratings. (The relationship between active power through the cable and maximum transmission distance, given a certain cable, will be discussed later.) For simplicity, it is further assumed that the rms value of line-to-line voltage at both sending and receiving ends is and the current through Z' and L_f is approximately equal to the current rating of the cable I_{reated}.

Since the ac filters are designed to supply all reactive power to the 12-pulse inverter at the sending end, the reactive power injected into the 20-Hz side of the cycloconverter can be estimated by using

$$Q_{\text{cyc}}^{20} \approx \text{Im}\{Y'\}V_c^2 + \omega_e 3C_f V_c^2 - 3I_{\text{rated}}^2\text{Im}\{Z'\} - 3I_{\text{rated}}^2\omega_e L_f \quad (18)$$

where the first two terms represent the reactive power generated from the cable and the capacitor of the *LC* filter, and the last two terms represent the reactive power consumed by the cable and the *LC* filter's inductor. The active power injected into the
cycloconverter from the 20-Hz side can be estimated by using

$$P_{\text{cyc}}^{20} \approx P_{\text{rated}} - \text{Re}\{Y'\}V_c^2 - 3I_{\text{rated}}^2\text{Re}\{Z'\} \quad (19)$$

where the last two terms represent the power loss of the cable.

The 20-Hz side power factor can be estimated according to (18) and (19).

The 60-Hz side power factor PF at the transformers' gridside terminals can be obtained using the 20-Hz power factor and the voltage ratio based on the analysis and calculations of ([30, p. 358]). Then, the apparent power rating of each of the three receiving-end transformers S_{tR} should satisfy

$$S_{tR} > \frac{P_{\text{cyc}}^{20}}{(3)(\text{PF}^{60})}. \quad (20)$$

Also, it is assumed that the grid-side ac filters are designed to supply the rated amount of reactive power to the cycloconverter.

3.2. Filter Design

At the sending end, the 12-pulse inverter produces harmonics of order m=12k±1,k=1,2.. , and can be represented as a source of harmonic currents (in Fig. 7). These current harmonics are filtered by two single-tuned filters for the 11th and 13th harmonic, and one damped filter for higher-order harmonics (> 23rd). Generally, the filter design is dependent on the reactive power supplied at fundamental frequency (also known as the filter size) and the required quality factor (QF) [32]. The total reactive power requirement of these filters can be estimated based on (15). Here, it is assumed that the total reactive power requirement is divided equally among the three filters. The quality factor for each filter can be determined using the method presented in ([32, Ch. 6]. A high quality factor 100) is used for the single-tuned filters, and a low quality factor(QF= 1) is used for the high-pass damped filter. Finally, with the capacitance and quality factor known, the inductance and resistance of each filter can be determined. With such filter design, the 12-pulse-related current harmonics originating at the sending end are essentially absent from the transmission line.

Fig. 7. Equivalent circuit of the LFAC transmission system for harmonic analysis. At the receiving end, there are two groups of filters, namely, the ac filters at the 60-Hz side and the *LC* filter at the 20-Hz side. At the 60-Hz side, if the cycloconverter generates exactly one-third of the grid frequency, and it can be shown [30, p. 360] that the line current has only odd harmonic components (3rd, 5th, 7th, etc). Subharmonic and interharmonic components are not generated. Here, three single-tuned filters and one damped filter are used to prevent these harmonic currents from being injected into the 60-Hz power grid. These filters are designed with a procedure similar to that for the ac filters at the sending end.

At the 20-Hz side, the line-to-neutral voltage has harmonics of order 3, 5, 7, , without subharmonic and interharmonic components [30, p. 306]. However, the harmonic components of order equal to integer multiples of three are absent in the line-to-line voltage. Therefore, as seen from the 20-Hz side, the cycloconverter acts as a source of harmonic voltages of orders n=6k±1,k=1,2.(in Fig. 7). The design of the *LC* filter has two objectives:

1) to decrease the amplitudes of the voltage harmonics generated by the cycloconverter; 2) to increase the equivalent harmonic impedance magnitudes seen from the receiving end, indicated by in Fig. 7.

The design procedure presented here takes into account the voltage harmonics of order 5, 7, 11, and 13. For cycloconverters, the amplitude of the voltage harmonics only depends on the voltage ratio and the fundamental power factor at the 20-Hz side, under the assumption of sinusoidal output current [30], which is sufficient for design purposes. Generally, the voltage harmonics tend to become worse with decreasing . Here, we set r=0.9. Fig. 8 illustrates the relationship between the per-unit amplitudes of the voltage harmonics under consideration and the power factor angle , computed based on formulas in [30, p. 303]. Apparently, for the 5th and 7th voltage harmonics, the amplitudes are symmetric with respect to φ=0 , and positive φ(i.e., reactive power consumption by the cycloconverter) can result in reduced amplitudes of the 11th and 13th voltage harmonics. At $\varphi=85^0$, minimum amplitudes are obtained. However, this value is unacceptably low, so $\varphi=35^0$ is selected (for operation at rated power).

After φ has been determined, it follows from (18) and (19) that there is a linear relation between Lf and Cf , as in Cf=aLf+b , since tan(φ) . However, any(Cf,Lf) pair determined based on this equation should only be used as an initial guess. These initial parameters might not yield the required power factor angle ($\varphi=35^0$) due to the simplifying assumptions made in the analysis. The proper *LC* filter parameters can be obtained by solving the circuit shown in Fig. 6.2 For example, given a value for Lf , the capacitance Cf that leads to the right power factor angle can be found by searching around its initial guess value. Therefore, if Lf varies within a certain range, a number of(Lf,Cf) pairs can be obtained. Among these(Lf,Cf) candidates, a selection is made such that the magnitudes|Zr(Wn)|for n=5,7,11,13 for are deemed to be adequately large. A numerical example will be provided in the next section.

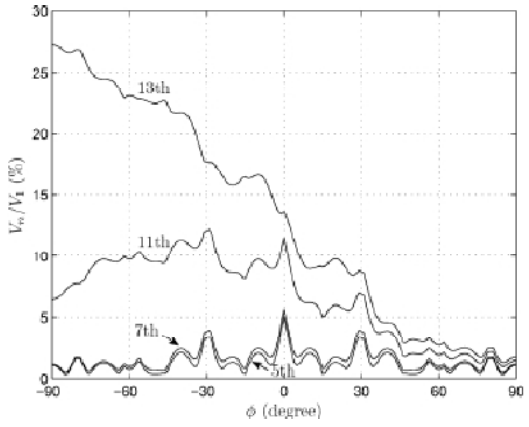

Fig. 8. Harmonic voltage amplitudes generated by the cycloconverter at the 20-Hz side.

4. Case Study

This section presents an example of the design process for a 20-Hz LFAC transmission system. The transmission voltage level is chosen as 132 kV. An appropriate submarine three-core XLPE power cable is selected (nominal voltage: 132 kV, maximum voltage: 145 kV, rated current: 825 A, cross section: 1000 mm , copper conductor). The cable's resistance, inductance, and capacitance are 17.6 m /km, 0.35 mH/km, and 0.25 F/km, respectively [33], [34].

The LFAC system is compared to a conventional 60-Hz HVAC transmission system that uses the same power cable, with a steady-state single-phase equivalent circuit shown in Fig. 9. The reactance Xac represents the short-circuit level of the 60-Hz power grid. Shunt reactive compensation and in Fig. 9) is connected at both ends to improve the active power transmission capability, especially for long transmission distances [35]. The power grid voltage is 132 kV line-to-line.
The short-circuit level is MVA, which is a typical value for a 132-kV system [36]. At the sending end, unity power factor is assumed , in order to calculate the maximum possible transmissible active power through the cable. Two cases are considered:

Case 1) No shunt reactive compensation, that is,$Xs=X_R$. This case is denoted as "60-Hz 0/0."
Case 2) Shunt reactive compensation split equally between the two ends. This case is denoted as "60-Hz 50/50." The total amount of reactive compensation is

The relationship between sending-end active power Ps and maximum transmission distance is calculated using the circuit of Fig. 9, and plotted in Fig. 10. The maximum transmission distance is obtained whenever the current or the voltage rating of the power cable is reached. In this case study, the cable's rated apparent power is 188 MVA. The maximum distance for transmitting 180 MW is 45 km without shunt compensation, and 70 km with shunt compensation. The 20-Hz LFAC system is designed to transmit 180 MW over 160 km. At the sending end, the dc bus voltage level is chosen as 30 kV. A 214-MVA, 132/13.2-kV (ns=10), 20-Hz phase-shift transformer is used. Due to the lower frequency, this transformer would be larger compared to a 60-Hz transformer.

This is a drawback of the proposed LFAC system. The total size of the ac filters at the sending end is 115 MVAr. For the cycloconverter, the voltage generated at the 20-Hz side is 132 kV (line-to-line). The voltage ratio is selected as r=0.9 , and the 20-Hz side power factor angle is designed to be $\varphi=35^0$. According to (4) and (5), the transformer ratio is nR= 1.5, and the 60-Hz side power factor is PF=.68 [30]. Based on the analysis of Section III-A and (20), the apparent power rating of each cycloconverter transformer is chosen to be 100 MVA. The total size of ac filters at the 60-Hz side is 200 MVAr.

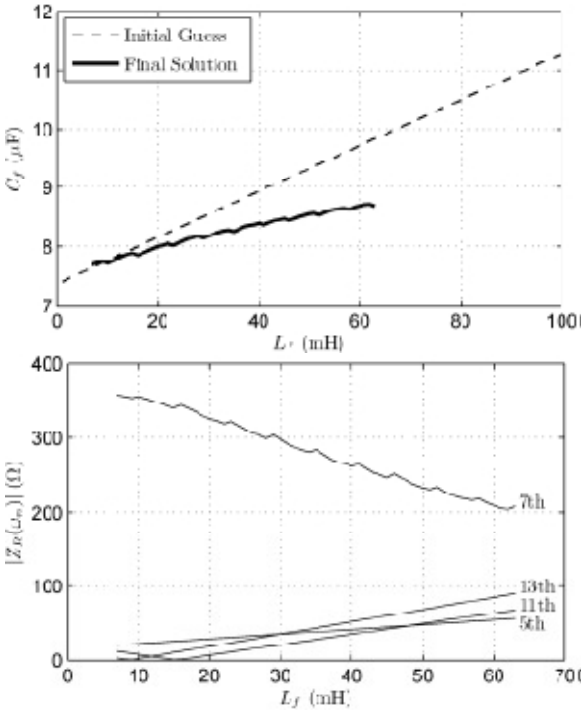

Fig. 11 depicts the approximate linear relation between Lf and Cf by a dashed line.

The more accurate capacitance values that yield the required power factor angle are represented by the solid curve. A solution can be found for values of Lf between 7 and 63 mH. Note that a solution can be obtained for Lf outside this range as well; however, in this case, either the current or the voltage rating of the power cable are violated. Fig. 12 shows the variation of |Zr(wn) |corresponding to the feasible (Lf,Cf) pairs. It can be seen that the *LC* filter with Lf= 63 mH and Cf= 8.7 F gives the maximum impedance magnitudes for the 5th, 11th, and 13th harmonics. Based on the aforementioned system parameters, the relationship between sending-end active power and maximum transmission distance for the 20-Hz LFAC system is calculated and superimposed in Fig. 10. It can be observed that the proposed LFAC system is a feasible option for delivering the rated power over a distance 2–3 times further than the HVAC solution.

Typically, for distances longer than 100 km, HVDC systems are the preferred solution [6], but an LFAC system could be an alternative transmission technology for the 100–200 km range, at least from a technical standpoint.

5. Simulation Results

To demonstrate the validity of the proposed LFAC system, simulations have been carried out using Matlab/Simulink and the Piecewise Linear Electrical Circuit Simulation (PLECS) toolbox [37]. The wind power plant is rated at 180 MW, and the transmission distance is 160 km. The system parameters are listed in Table I. The parameters of the PI controllers in Figs. 2 and 3 are listed in Table II. The transmission power cable is modeled by cascading 20 identical sections. The ABB 5STP 42U6500 [38] and the ABB 5STP 08F6500 [39] thyristors are selected to construct the sending-end inverter and the receiving-end cycloconverter, respectively. Multiple series-connected thyristors (5 thyristors at the sending end and 30 thyristors at the receiving end) are used such that the rated voltage of a switch is 150% of the rated blocking voltage. Fig. 13 shows the steady-state line-to-line voltage and current waveforms at the sending end, the receiving end, the 20-Hz side of the cycloconverter, and the 60-Hz power grid side under rated power conditions. The 20-Hz voltage generated from the cycloconverter has significant harmonic distortion (THD is 14.8%).

Due to the *LC* filter, the voltages at the receiving and sending ends have reduced THD values (3.9% and 2.2%, respectively). The measured fundamental power factor side of the cycloconverter is 34.9 , which is close to the design requirement. Fig. 14 depicts the results of a transient simulation where the power from the wind turbines ramps from 0 to 180 MW, at a rate of 60 MW/s (perhaps unrealistically fast, but chosen to demonstrate that the system is stable even for this large transient). Shown are the transient responses of the dc bus voltage at the sending end, the magnitude of the fundamental component of the 20-Hz voltage generated by the cycloconverter power injected into the 60-Hz power grid, and the transmission efficiency (which reaches a value of 93.3% at rated power).

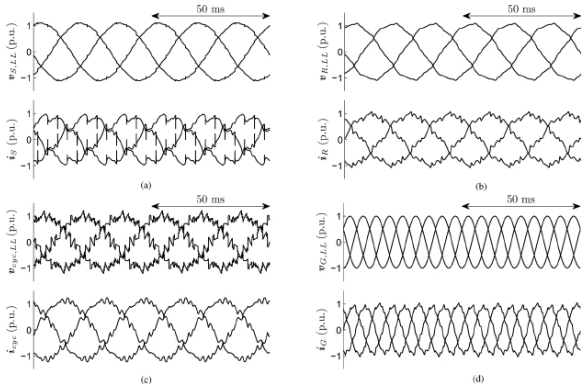

Fig. 13. Simulated voltage and current waveforms. (Please refer to Fig. 1 for voltage and current monitoring positions.) (a) Sending end. (b) Receiving end. (c) Cycloconverter 20-Hz side. (d) 60-Hz power grid side

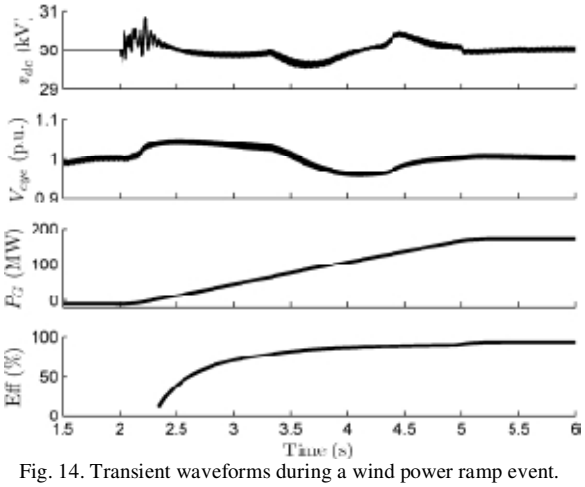

Fig. 14. Transient waveforms during a wind power ramp event.

6. Conclusion

A low-frequency ac transmission system for offshore wind power has been proposed. A method to design the system's components and control strategies has been discussed. The use of a low frequency can improve the transmission capability of submarine power cables due to lower cable charging current. The proposed LFAC system appears to be a feasible solution for the integration of offshore wind power plants over long distances, and it might be a suitable alternative over HVDC systems in certain cases. Furthermore, it might be easier to establish an interconnected low-frequency ac network to transmit bulk power from multiple plants. In order to make better-informed decisions, it is necessary to perform a complete technical and eco- Fig. 14. Transient waveforms during a wind power ramp event. side of the cycloconverter is 34.9 , which is close to the design requirement. Fig. 14 depicts the results of a transient simulation where the power from the wind turbines ramps from 0 to 180 MW, at a rate of 60 MW/s (perhaps unrealistically fast, but chosen to demonstrate that the system is stable even for this large transient). Shown are the transient responses of the dc bus voltage at the sending end, the magnitude of the fundamental component of the 20-Hz voltage generated by the cycloconverter, the active nomic comparison among HVAC, HVDC, and LFAC, evaluating factors, such as the transmission efficiency, investment and operating costs, and the performance under system transients.

References

[1] National Grid Electricity Transmission, London, U.K., 2011 offshore development information statement, Tech. Rep., Sep. 2011. [Online]. Available: http://www.nationalgrid.com/uk/Electricity/OffshoreTransmission/ODIS/Current Statement/

[2] T. Mai, R. Wiser, D. Sandor, G. Brinkman, G. Heath, P. Denholm, D.J. Hostick, N. Darghouth, A. Schlosser, and K. Strzepek, "Exploration of high-penetration renewable electricity futures study," National Renewable Energy Laboratory, Golden, CO, Tech. Rep. NREL/TP-6A20- 52409-1, National Renewable Energy Laboratory.

[3] N. B. Negra, J. Todorovic, and T. Ackermann, "Loss evaluation of HVAC and HVDC transmission solutions for large offshore wind farms," *Elect. Power Syst. Res.*, vol. 76, no. 11, pp. 916–927, Jul. 2006.

[4] S. Bozhko, G. Asher, R. Li, J. Clare, and L. Yao, "Large offshore DFIGbased wind farm with line-commutated HVDC connection to the main grid: Engineering studies," *IEEE Trans. Energy Convers.*, vol. 23, no. 1, pp. 119–127, Mar. 2008.

[5] O. Gomis-Bellmunt, J. Liang, J. Ekanayake, R. King, and N. Jenkins, "Topologies of multiterminal HVDC-VSC transmission for large offshore wind farms," *Elect. Power Syst. Res.*, vol. 81, no. 2, pp. 271–281, Feb. 2011.

[6] P. Bresesti, W. L. Kling, R. L. Hendriks, and R. Vailati, "HVDC connection of offshore wind farms to the transmission system," *IEEE Trans. Energy Convers.*, vol. 22, no. 1, pp. 37–43, Mar. 2007.

[7] S. V. Bozhko, R. Blasco-Giménez, R. Li, J. C. Clare, and G. M. Asher, "Control of offshore DFIG-based wind farm grid with line-commutated HVDC connection," *IEEE Trans. Energy Convers.*, vol. 22, no. 1, pp. 71–78, Mar. 2007.

[8] J. Arrillaga, *High Voltage Direct Current Transmission*, 2nd ed. London, U.K.: Institution of Electrical Engineers, 1998.

[9] N. Flourentzou, V. G. Agelidis, and G. D. Demetriades, "VSC-based HVDC power transmission systems: An overview," *IEEE Trans. Power Electron.*, vol. 24, no. 3, pp. 592–602, Mar. 2009.

[10] T. Funaki and K. Matsuura, "Feasibility of the lower frequency AC transmission," in *Proc. IEEE Power Eng. Soc. Winter Meeting*, 2000, vol. 4, pp. 2693–2698.

[11] X. Wang, C. Cao, and Z. Zhou, "Experiment on fractional frequency transmission system," *IEEE Trans. Power Syst.*, vol. 21, no. 1, pp. 372–377, Feb. 2006.

[12] N. Qin, S. You, Z. Xu, and V. Akhmatov, "Offshore wind farm connection with low frequency ac transmission technology," presented at the IEEE Power Energy Soc. Gen. Meeting, Calgary, AB, Canada, 2009.

[13] Y. Cho, G. J. Cokkinides, and A. P. Meliopoulos, "Time domain simulation of a three-phase cycloconverter for LFAC transmission systems," presented at the IEEE Power Energy Soc. Transm. Distrib. Conf. Expo., Orlando, FL, May 2012.

[14] M. Liserre, R. Cárdenas, M. Molinas, and J. Rodríguez, "Overview of multi-MW wind turbines and wind parks," *IEEE Trans. Ind. Electron.*, vol. 58, no. 4, pp. 1081–1095, Apr. 2011.

[15] C. Meyer, M. Höing, A. Peterson, and R. W. De Doncker, "Control and design of DC grids for offshore wind farms," *IEEE Trans. Ind. Appl.*, vol. 43, no. 6, pp. 1475–1482, Nov./Dec. 2007.

[16] S. Lundberg, "Evaluation of wind farm layouts," presented at the Nordic Workshop Power Ind. Electron., Trondheim, Norway, Jun. 2004.

[17] J. Yang, J. Fletcher, and J. O'Reilly, "Multiterminal DC wind farm collection grid internal fault analysis and protection design," *IEEE Trans. Power Del.*, vol. 25, no. 4, pp. 2308–2318, Oct. 2010.

[18] J. Robinson, D. Jovcic, and G. Joós, "Analysis and design of an offshore wind farm using a MV DC grid," *IEEE Trans. Power Del.*, vol. 25, no. 4, pp. 2164–2173, Oct. 2010.

[19] D. Jovcic, "Offshore wind farm with a series multiterminal CSI HVDC," *Elect. Power Syst. Res.*, vol. 78, no. 4, pp. 747–755, Apr. 2008.

[20] A. Prasai, J.-S. Yim, D. Divan, A. Bendre, and S.-K. Sul, "A new architecture for offshore wind farms," *IEEE Trans. Power Electron.*, vol. 23, no. 3, pp. 1198–1204, May 2008.

[21] S. Nishikata and F. Tatsuta, "A new interconnecting method for wind turbine/generators in a wind farm and basic performances of the integrated system," *IEEE Trans. Ind. Electron.*, vol. 57, no. 2, pp. 468–475, Feb. 2010.

[22] M. Popat, B. Wu, F. Liu, and N. Zargari, "Coordinated control of cascaded current-source converter based offshore wind farm," *IEEE Trans. Sustain. Energy*, vol. 3, no. 3, pp. 557–565, Jul. 2012.

[23] M. H. Johnson, H. Chen, and D. C. Aliprantis, "Offshore wind farm with c collection system," presented at the IEEE Power Energy Conf., Urbana, IL, Feb. 2013.

[24] E. Prieto-Araujo, F. D. Bianchi, A. Junyent-Ferré, and O. Gomis-Bellmunt, "Methodology for droop control dynamic analysis of multiterminal VSC-HVDC grids for offshore wind farms," *IEEE Trans. Power Del.*, vol. 26, no. 4, pp. 2476–2485, Oct. 2011.

[25] E. Veilleux and B. Ooi, "Multiterminal HVDC with thyristor power-flow controller," *IEEE Trans. Power Del.*, vol. 27, no. 3, pp.1205–1212, Jul. 2012.

[26] B. K. Bose, *Modern Power Electronics and AC Drives*. Upper Saddle River, NJ: Prentice-Hall, 2002.

[27] J. Arrillaga, Y. H. Liu, and N. R. Watson, *Flexible Power Transmission: The HVDC Options*. Hoboken, NJ: Wiley, 2007.

[28] B. Wu, *High-Power Converters and AC Drives*. Hoboken, NJ: Wiley, 2006.

[29] P. C. Krause, O. Wasynczuk, and S. D. Sudhoff, *Analysis of Electric Machinery and Drive Systems*, 2nd ed. Piscataway, NJ: IEEE, 2002.

[30] B. R. Pelly, *Thyristor Phase-Controlled Converters and Cycloconverters*. New York: Wiley, 1971.

[31] A. R. Bergen and V. Vittal, *Power System Analysis*, 2nd ed. Upper Saddle River, NJ: Prentice-Hall, 2000.

[32] J. Arrillaga and N. R. Watson, *Power System Harmonics*, 2nd ed. Chichester, U.K.: Wiley, 2003.

[33] *"XLPE Land Cable Systems User's Guide."* [Online]. Available: http:// www.abb.com

[34] ABB, XLPE submarine cable systems. [Online]. Available:http://www.abb.com

[35] National Grid Electricity Transmission plc., London, U.K., 2010 offshore development information statement, Tech. Rep., Sep. 2010. [Online]. Available: http://www.nationalgrid.com/uk/Electricity/ ODIS/Archive/

[36] L. Freris and D. Infield, *Renewable Energy in Power Systems*.Hoboken, NJ: Wiley, 2008.

[37] *"PLECS User Manual,"* [Online]. Available: http://www.plexim.com/ downloads/

[38] 5STP 42U6500 data sheet. [Online]. Available: http://www.abb.com/ ProductGuide/

[39] 5STP 08F6500 data sheet. [Online]. Available: http://www.abb.com/ ProductGuide